BIOLOGY OF REPRODUCTION (2016) **95**(6):127, 1–11
Published online before print 19 October 2016.
DOI 10.1095/biolreprod.116.142257

# Phospholipid Profile and Distribution in the Receptive Oviduct and Uterus During Early Diestrus in Cattle[1]

**Katia Roberta A. Belaz,[3,4] Alessandra Tata,[4] Moana R. França,[5] Maressa I. Santos da Silva,[5] Pedro Henrique Vendramini,[4] Anna Maria A.P. Fernandes,[4] Fábio L. D'Alexandri,[5] Marcos N. Eberlin,[4] and Mario Binelli[2,5]**

*[4]ThoMSon Mass Spectrometry Laboratory, Institute of Chemistry, University of Campinas, UNICAMP, Campinas, Brazil*
*[5]School of Veterinary Medicine and Animal Science, University of São Paulo, Pirassununga, Brazil*

## ABSTRACT

**Phospholipid metabolism and signaling influences on early pregnancy events in cattle are unknown. This study aimed to characterize global phospholipid composition of oviduct and uterus during early diestrus in a model of contrasting embryo receptivity. Beef cows were treated to ovulate a larger (LF-LCL group, associated with greater receptivity) or smaller (SF-SCL group) follicle and, consequently, to present greater or smaller plasma concentrations of estradiol during proestrus-estrus, as well as progesterone during early diestrus. Oviduct and uterus (4 days after gonadotropin-releasing hormone-induced ovulation; D4) as well as the uterus (D7) were collected, and lipid profiles were monitored by matrix-assisted laser desorption/ionization mass spectrometry (MALDI-MS). This technique allowed the identification and tissue localization of sphingomyelins (SM), phosphatidylcholines (PC), ceramides (Cer), and phosphatidylethanolamines (PE). Multivariate statistics were used to separate samples into groups with distinctly different phospholipid profiles in the uterus at D4 and D7. Different abundance of ions corresponding to specific lipids were detected on D4 (Cer [42:1], PC [31:0], PC [32:1], PC [34:4], and PC [36:4] greater for LF-LCL group; and PC [38:7], PC [38:5], PC [38:4], PC [40:7], and PC [40:6] greater for SF-SCL group) and D7 (SM [34:2], SM [34:1], PC [32:1], and PC [35:2] greater for LF-LCL group). The MALDI-MS imaging showed the spatial distributions of major phospholipids. In conclusion, distinct phospholipid profiles were associated with animals treated to show contrasting receptivity to the embryo. Functional roles of the identified phospholipids on uterine function and preimplantation embryo development deserve further studies.**

*lipidomics, MALDI-MS, mass spectrometry, oviduct, sex steroids, uterus*

## INTRODUCTION

Low reproductive efficiency is a major worldwide constraint to the production of cattle meat and milk. Major causes of such reproductive failure are embryonic and fetal losses [1]. Successful establishment of pregnancy depends on a delicate balance between luteolytic mechanisms inherent to the endometrium at the end of the estrous cycle and antiluteolytic mechanisms, orchestrated by the conceptus, to change endometrial function to ultimately block luteolysis [2]. Hormonal, as well as pharmacological, nutritional, and mechanical manipulation of the estrous cycle in artificial insemination programs aims to maximize the odds of pregnancy. For example, the increase in progesterone concentrations during diestrus has been found to positively affect fertility [3, 4].

The role of progesterone in regulating uterine function and embryo development [5], as well as strategies to increase pregnancy rates based on the increase of its concentrations, were reviewed recently [2, 6, 7]. Interestingly, Demetrio et al. [8] demonstrated a positive relationship between progesterone concentrations at Day 7 (D7) after estrus and the probability of pregnancy at D28 after insemination of dairy cows. Similar results were reported for inseminated beef cows [9, 10] and embryo transfer recipients [11]. We have characterized an animal model that modulates the periovulatory sex steroid milieu in beef cattle [12]. In this model, animals that ovulate larger follicles (i.e., the large follicle-large corpus luteum [LF-LCL] group) present greater proestrus-estrus concentrations of estradiol (E2) and diestrus concentrations of progesterone (P4) compared with cows that ovulate smaller follicles (the small follicle-small CL [SF-SCL] group). In a fertility trial, the proportion of cows pregnant between D35 and D40 after artificial insemination in the LF-LCL group was also greater than that of the SF-SCL group [4]. The endometrial transcriptome measured on D7 of the estrous cycle was also distinctly different between the two groups [13]. Most importantly, such changes in the transcriptome were reflected in different proliferative [13] and redox uterine phenotypes between groups [14]. In contrast to transcriptomic information, which has been reported extensively, information on global metabolite and lipid composition in the reproductive tract, in association with receptivity, is missing. Here, we report the association between phospholipid metabolism and signaling on reproductive tract receptivity, using the animal model of high or low fertility described by Mesquita et al. [12].

[1]Supported by São Paulo Research Foundation FAPESP grants 2012/07206-0, 2011/06191-7, 2011/03226-4, and 2013/19620-9; and by the Conselho Nacional de Desenvolvimento Científico e Tecnológico (CNPq) and the Coordination for the Improvement of Higher Education Personnel (CAPES).
[2]Correspondence: Mário Binelli, School of Veterinary Medicine and Animal Science, University of São Paulo, 13635-900, Pirassununga-SP, Brazil. E-mail: binelli@usp.br
[3]Correspondence: Katia Roberta A. Belaz, ThoMSon Mass Spectrometry Laboratory, Institute of Chemistry, University of Campinas-UNICAMP, 13084-971, Campinas-SP, Brazil. E-mail: robertabelaz@yahoo.com.br

Received: 28 May 2016.
First decision: 18 July 2016.
Accepted: 6 October 2016.

eISSN: 1529-7268 http://www.biolreprod.org
ISSN: 0006-3363

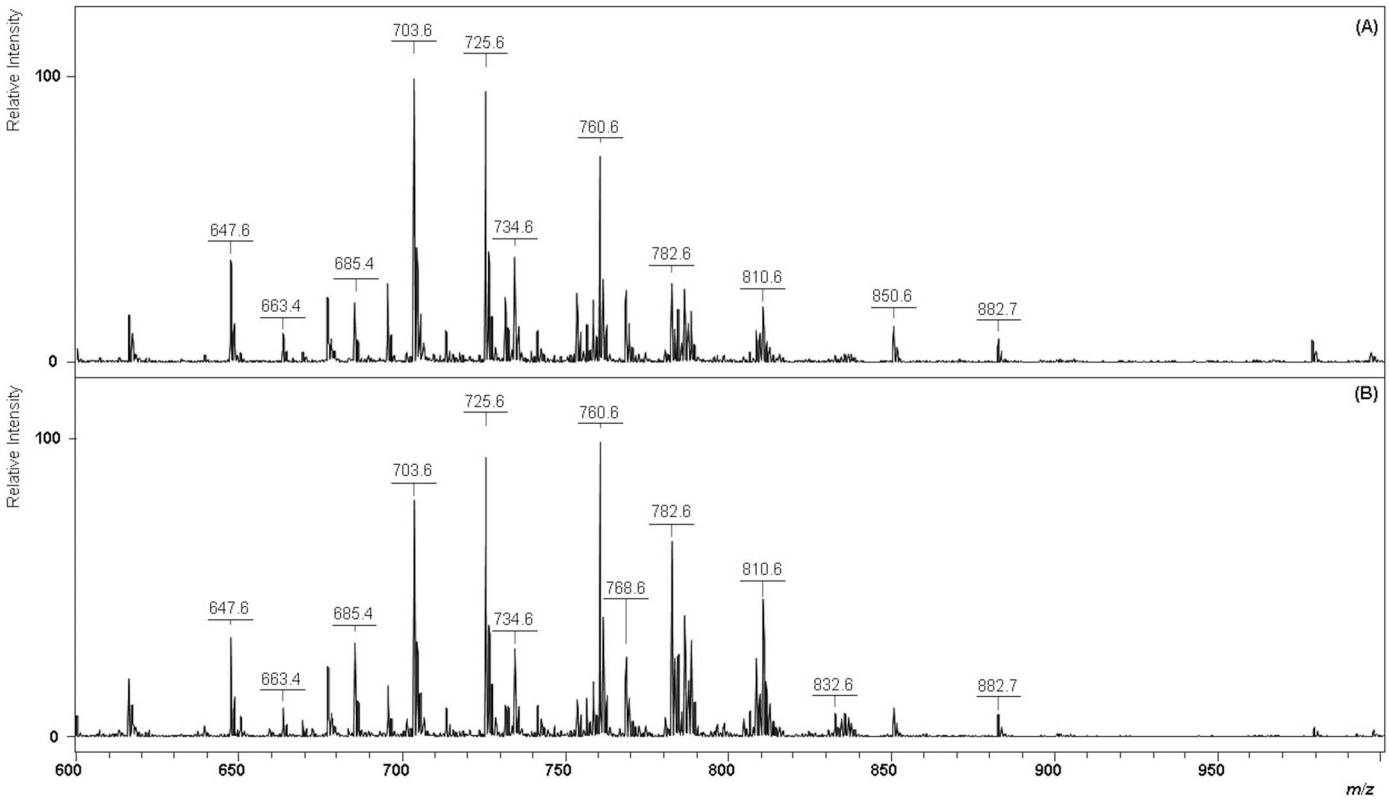


FIG. 1. Representative MALDI(+)-MS of oviducts of LF-LCL (**A**) and SF-SCL (**B**) cows at D4 of the estrous cycle. The x-axis represents the *m/z* values of lipid ions, whereas the y-axis reports the relative abundance of each ion expressed as a percentage to the most abundant ion.

Phospholipids are vital metabolites that function as structural and regulatory components of biological membranes and serve as precursors to many biomolecules, such as eicosanoids and lysophospholipids [15, 16]. A study by Meier et al. [17] examined changes in uterine endometrial phospholipids and fatty acids throughout the estrous cycle and early pregnancy in the ewe. Their results indicate that endometrial lipid abundance increased as the estrous cycle progressed from D3 to D12 and then to D15, whereas during early pregnancy, endometrial lipid concentrations decreased on D15 of pregnancy compared with D3 and D12. Phosphatidylcholines (PC) followed a similar pattern to that of total phospholipids, with an increase in PC concentrations as the estrous cycle progressed. Similar studies have never been conducted in the cow. Specifically, there have been no attempts to associate lipid profiles of the reproductive tract and receptivity phenotypes.

Here, we used matrix-assisted laser desorption ionization-mass spectrometry (MALDI-MS) to investigate changes in the lipid composition of the uterus and oviducts at D4 and that of the uterus alone on D7 from cows treated to present greater (LF-LCL) or lower (SF-SCL) receptivity phenotypes. We hypothesized that within each organ and day investigated, lipid profiles are different between groups. The MALDI-MS was applied because it has gained widespread use in this field due to its unlimited molecular weight (MW) coverage in addition to several other advantages, such as high tolerance to salts and impurities, simple spectra, rapid analysis, and relatively easy instrumentation [18]. In the field of animal reproduction, MALDI-MS has also been applied to reveal lipid profiles of single embryos [19, 20], oocytes [21] and blastocysts [22], and spermatozoa from human, Ruminantia, and Feloidea species [23–25]. Such profiles have allowed the discrimination of different mammalian species through the detection of sphingomyelins (SMs), PC, and triacylglycerols. Recently, spatial and temporal alterations of phospholipid composition during mouse embryo implantation were monitored by MALDI-MS, showing the importance of the complex interplay of lipid molecules in uterine biology during implantation [26]. Complementary to MALDI MS, accurate *m/z* measurement of the lipid ions was performed by high-resolution mass spectrometry (HRMS) using an electrospray orbitrap mass spectrometer (ESI-Orbitrap-MS) in order to increase the quality of lipid identification. Multivariate statistics via principal component analysis (PCA) and orthogonal partial least square (OPLS) were also applied to interpret the MALDI-MS data set. Also for the first time in the uterus, tissue compartment-specific localization of selected phospholipids was mapped by MALDI-MS imaging.

## MATERIALS AND METHODS

### Reagents

Unless stated otherwise, all of the chemicals used were purchased from Sigma Chemical Co.

### Animals, Reproductive Management, and Experimental Design

Animal procedures were approved by the Ethics and Animal Handling Committee of the University of São Paulo (protocol 2280/2011). The experiments were conducted at the University of São Paulo, Pirassununga, Brazil. Pluriparous, cycling, nonlactating Nelore (*Bos indicus*) cows were used. Females did not present detectable reproductive disorders, as evaluated by transrectal palpation and ultrasonography conducted by experienced veterinarians.

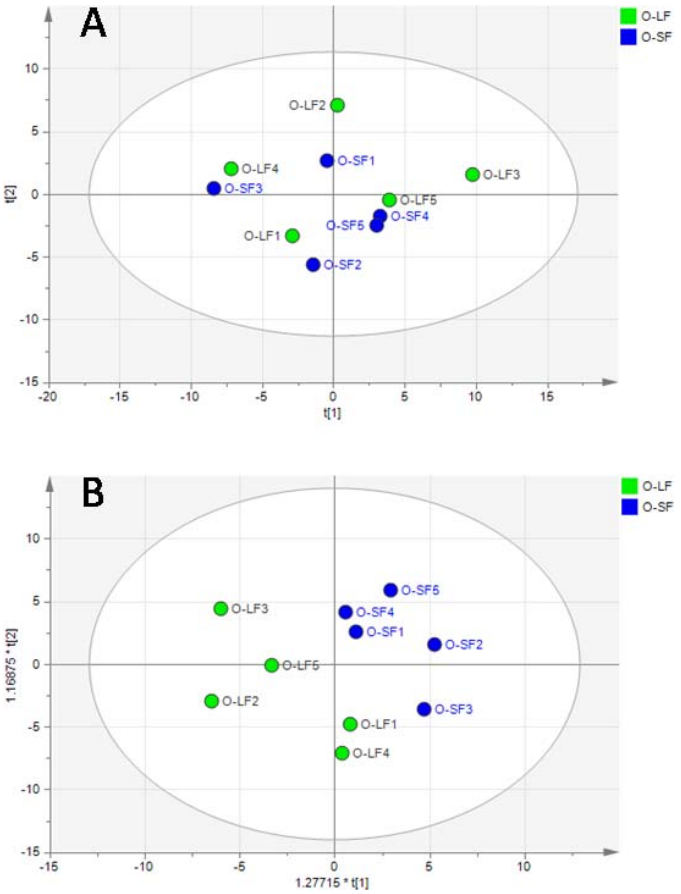


FIG. 2. A PCA (**A**) and an OPLS (**B**) plot of the MALDI(+)-MS data obtained from oviducts of cows at D4 of the estrous cycle. Each colored dot represents an individual animal of the LF-LCL (O-LF; green) or SF-SCL (O-SF; blue) group. No discrimination of the two groups was observed ($R^2 = 0.19$) by PCA. **B**) Weak separation of the two groups was observed by OPLS ($R^2 = -0.60$; $Q^2 = 0.82$).

A hormonal protocol was applied to control follicle growth, aiming to produce groups of animals with distinctly different preovulatory follicle sizes, plasma concentrations of estradiol, and early diestrus concentrations of progesterone, as published previously by Mesquita et al. [12]. Briefly, cows received two intramuscular (IM) injections of prostaglandin F2α (PGF2α; 0.5 mg; sodium cloprostenol; Sincrocio; Ourofino) 14 days apart. Following this presynchronization procedure, the ovaries were visualized using transrectal ultrasound scanning to confirm the presence of a PGF-responsive CL 10 days after the second PGF administration, (D−10 of the experiment). On D−10, all cows were treated with 2 mg of estradiol benzoate (Sincrodiol; Ourofino) and received an intravaginal P4-releasing device (1 mg; Sincrogest; Ourofino) to promote the emergence of a new follicular wave. Also, on D−10, the animals from the LF-LCL group received another IM administration of PGF (0.5 mg; sodium cloprostenol) to promote CL regression and to decrease the circulating P4 level during follicular growth. Sixty hours prior to the induction of ovulation, the P4 devices were removed, and a PGF dose (0.5 mg; sodium cloprostenol) was administered IM to the cows in the LF-LCL group, whereas the cows in the SF-SCL group received the same treatment 12 h later (D2.5 and D2, respectively). Ovulation was induced on D0 by IM administrations of gonadotropin-releasing hormone (GnRH; 1 μg of buserelin acetate; Sincroforte; Ourofino). Animals were evaluated by transrectal ultrasonography every 24 h starting on D2. Blood samples were collected by puncture of the jugular vein using 10-ml vials containing heparin for analysis of P4 concentrations. Plasma was harvested by centrifugation (4°C and 1500 × *g* for 30 min) and stored at −20°C. Endocrine and ovarian data were reported previously [12, 13, 27].

In experiment 1, animals from each group (LF-LCL, n = 7; or SF-SCL, n = 7) were slaughtered on D4 post-GnRH treatment, and the reproductive tracts were removed, placed immediately on ice, and dissected within 20 min of collection. Uterus and oviducts were obtained from each cow. On a styrofoam box containing liquid nitrogen, cross sections of the cranial tip of each uterine horn were secured at 3 cm from the liquid nitrogen surface for approximately 15 min and subsequently stored at −80°C. Using a similar method, the oviduct of each animal was collected and a cross section of the midportion of the ampullar region was frozen in liquid nitrogen vapor and stored at −80°C. For the sake of simplicity, the ampullar region of the oviduct is called ''oviduct'' hereafter in this paper. Only uterus and oviducts obtained from the uterine horn ipsilateral to the ovary containing the CL were used for the subsequent analyses. Cross-sectional samples were used both for the MALDI-MS analyses and for the MALDI-MS imaging analyses.

In experiment 2, animals from each group (LF-LCL, n = 7; or SF-LCL, n = 10) were slaughtered on D7 after GnRH treatment; samples from the uterus were collected and stored as described for experiment 1.

## Lipid Profile Analysis by MALDI-MS

*Sample preparation*. Samples were subjected to liquid-liquid extraction of the total lipids following the protocol described by Bligh and Dyer (BD) [28]. From each sample of either the oviduct or the uterus, a 1-mm-thick cross section, including all tissue layers, was cut with a blade and added to individual microcentrifuge tubes. Volumes of 150 μl of water, 190 μl of methanol, and 370 μl of chloroform were added, and then the tubes were shaken vigorously for 2 min. Subsequently, samples were centrifuged for 5 min at 13 000 × *g*, the aqueous supernatant was discarded, and the organic phase (lower phase) was collected and dried for 40 min in a concentrator. Samples were resuspended in 50 μl of a mixture MeOH:$CHCl_3$ (1:1).

Each sample of extract (1 μl) was placed on a spot on the MALDI target plate, allowed to dry at room temperature, and covered with 1 μl of 30.0 mg/ml 2,5-dihydroxybenzoic acid (DHB) diluted in methanol just before analysis.

*MALDI-MS data acquisition*. The MALDI-MS data were acquired using an Autoflex III MALDI time-of-flight mass spectrometer operated in the reflectron mode (BrukerDaltonics) and equipped with a 337-nm smart beam laser. The MS data were acquired in the positive ion mode and in the *m/z* 600–1000 range by averaging 800 consecutive laser shots at a frequency of 200 Hz. FlexAnalysis 3.0 software (BrukerDaltonics) was used to process the mass spectra. The most abundant ions from each spectrum (that were clearly distinct from noise after the exclusion of isotopic peaks) were considered a starting point in the search for *m/z* values corresponding to lipids; these abundant ions were submitted to statistical analysis.

## Accurate m/z Measurements and Lipid Ion Assignments

Samples were run in the Q-Exactive Mass Spectrometer (Thermo Fisher Scientific) using electrospray ionization (ESI). The Q-Exactive mass spectrometer is a stand-alone Orbitrap used to analyze the chemical composition of the lipid ions with high accuracy due to its high resolution (140 000@400) and ppb accuracy. The BD extracts (analyzed previously by MALDI[+]-MS) were diluted 10-fold in an MeOH:$H_2O$ (1:1; 0.1% formic acid) solution and again analyzed by ESI(+)-Orbitrap-MS. The MS and MS/MS experiments were used to identify the lipid ions via elemental compositions and dissociation chemistry. Accurate experimental *m/z* values were compared to the exact mass using a database search at http://www.lipidmaps.org. A match between the experimental *m/z* value and theoretical *m/z* value from the library was considered when the mass error was <3.1 ppm.

## MALDI MS Imaging

Uterine sections of 20-μm thickness were prepared using a cryomicrotome (CM1850; Leica), thaw-mounted onto ITO-coated MALDI plates, and stored at −80°C. Prior to MALDI-MS imaging, tissue sections were placed inside a vacuum desiccator for 8 min to remove the excess of water. The DHB matrix was prepared at a concentration of 30 mg/ml in methanol, and 10 ml of the solution was applied to the section with airbrush at 15-cm plate distance. Tissue sections were analyzed by MALDI-MS imaging using the same instrument described in the previous section. The MALDI-MS imaging experiment was set up by the program FlexImaging 4.0 (BrukerDaltonics). The laser diameter was set to 50 μm and tracked along the x- and y-axis of selected regions at 100-μm spatial resolution. Each spectrum was acquired as an average of 800 laser shots on a single spot. Images were generated and normalized using the FlexImaging software. The normalization used was root mean square. An adjacent section of uterus was sliced with a thickness of 10 μm and subjected to hematoxylin-eosin staining.

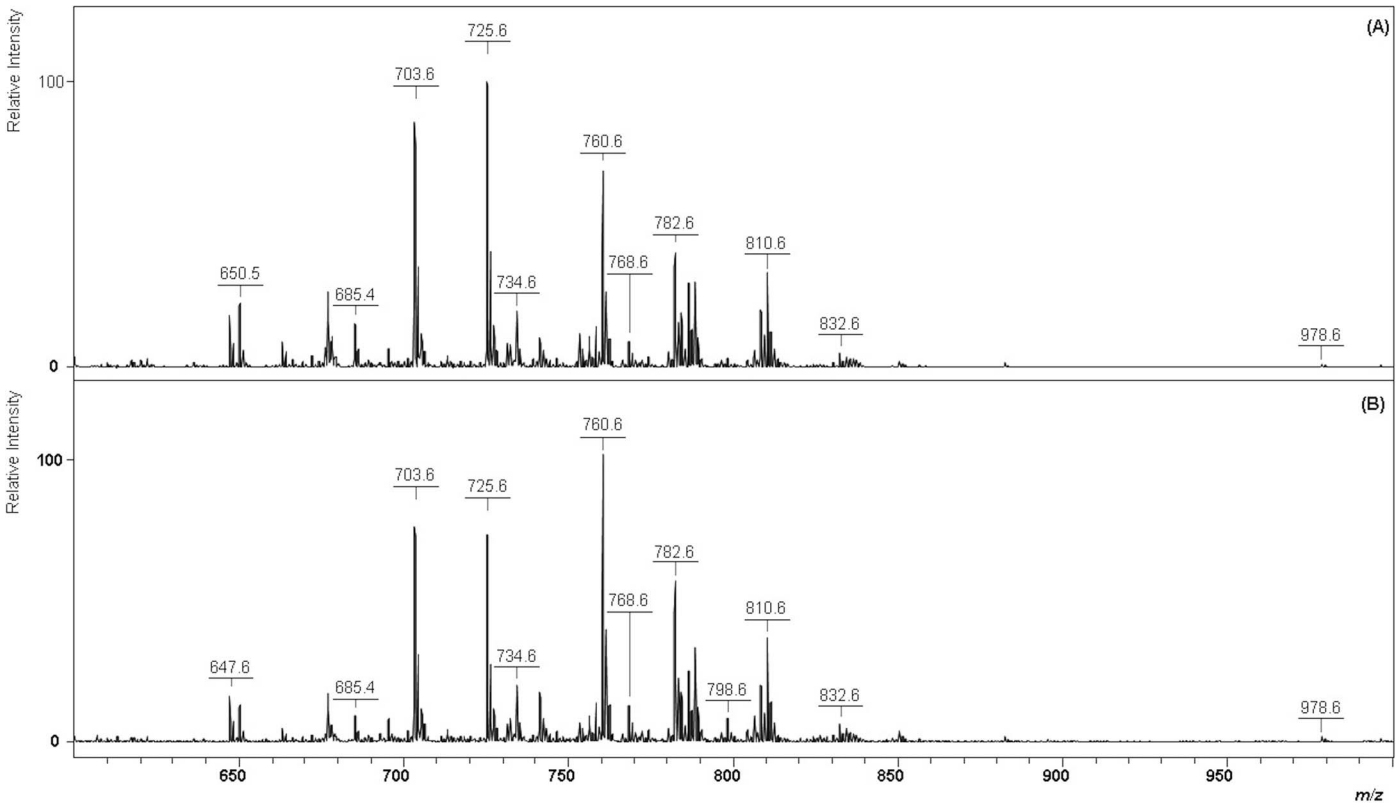


FIG. 3. Representative MALDI(+)-MS of uterus of LF-LCL (**A**) and SF-SCL (**B**) cows at D4 of the estrous cycle. The x-axis represents the *m/z* values of lipid ions, whereas the y-axis reports the relative abundance of each ion expressed as a percentage to the most abundant ion.

### *Statistical Analysis*

Multivariate data analyses using PCA and OPLS were performed using SIMCA-P+ 12 (Umetrics) following log transformation, mean centering and UV-scaling. Model performance was reported as cumulative correlation coefficients for the model (R2X [cum] or R2Y [cum]) and predictive performance was based on cross validation calculations (Q2 [cum]) and CV-ANOVA. Univariate statistical analysis was performed using Student's unpaired *t*-test. Boxplot graphs were generated to represent the ions distributions in the samples by using Prism 5 GraphPad Inc. software.

## RESULTS

### *Ovarian and Endocrine Responses*

Endocrine and ovarian data have been published previously [12, 13, 27]. Briefly, for the animals slaughtered on D4, preovulatory follicle size and plasma E2 concentration on D −1, and plasma concentration of P4 on D4 (mean ± SEM) were 15.70 ± 0.43 versus 11.31 ± 0.23 mm ($P < 0.01$), 2.44 ± 0.19 versus 0.65 pg/ml ($P < 0.01$), and 1.40 ± 0.23 versus 0.80 ± 0.10 ng/ml ($P < 0.01$) for the LF-LCL versus SF-SCL groups, respectively. For the animals slaughtered on D7, preovulatory follicle size on D0, plasma E2 concentration on D −1, and plasma P4 concentration on D7 (mean ± SEM) were 13.18 ± 0.44 versus 10.63 ± 0.30 mm ($P < 0.01$), 2.30 ± 0.57 versus 0.50 ± 0.13 pg/ml ($P < 0.01$), and 3.68 ± 0.38 versus 2.49 ± 0.43 ng/ml ($P = 0.04$) for the LF-LCL versus SF-SCL groups, respectively. Such differences in dominant follicle size and hormonal profiles clearly indicate that experimental groups presented distinctly different periovulatory endocrine milieus.

### *Experiment 1: Lipid Profile of Oviduct and Uterus at D4*

*Oviducts D4*. The lipid profile of the oviduct tissue of LF-LCL or SF-SCL cows at D4 of the estrous cycle was determined by MALDI-MS. Representative MALDI spectra for each experimental group are shown in Figure 1. The lipid profile of the bovine oviduct at D4 of the estrous cycle is characterized by the major ions of *m/z* 647.6, 663.4, 650.5, 703.5, 725.5, 732.5, 758.6, 760.6, 780.6, 782.6, 786.6, 788.6, 808.6, 810.6, 850.6, and 882.7. Subsequently, MALDI-MS data were explored by multivariate analysis (Fig. 2) to investigate differences between the experimental groups.

The PCA of the MALDI-MS data set was performed to verify the data distribution. The PCA allows the projection of higher-dimensional data onto a lower-dimensional space. When PCA is applied to a set of data, samples with similar trends in their ion profiles tend to cluster close together. The R2 parameter indicates how well the model explains the current data set. As shown in the score plot of the PCA model (Fig. 2A), constructed with two principal components, no discrimination of the two groups was achieved (R2 [cum] = 0.19). Next, an OPLS model was used to measure the multidimensional association of the lipid profile of the tissue with the endocrine phenotype provided by the biological model (i.e., LF-LCL vs. SF-SCL). Besides the R2, another parameter, named Q2, was used to describe the OPLS model. The Q2 represents the correlation, based on averaged results of repeated iterations, to cross-validation. As such, the Q2 represents a measure of the predictive power of the model. In the OPLS model, values calculated were R2 [cum] = −0.60 and Q2 [cum] = 0.82. The model was built from a single predictive and one orthogonal component and resulted in a weak

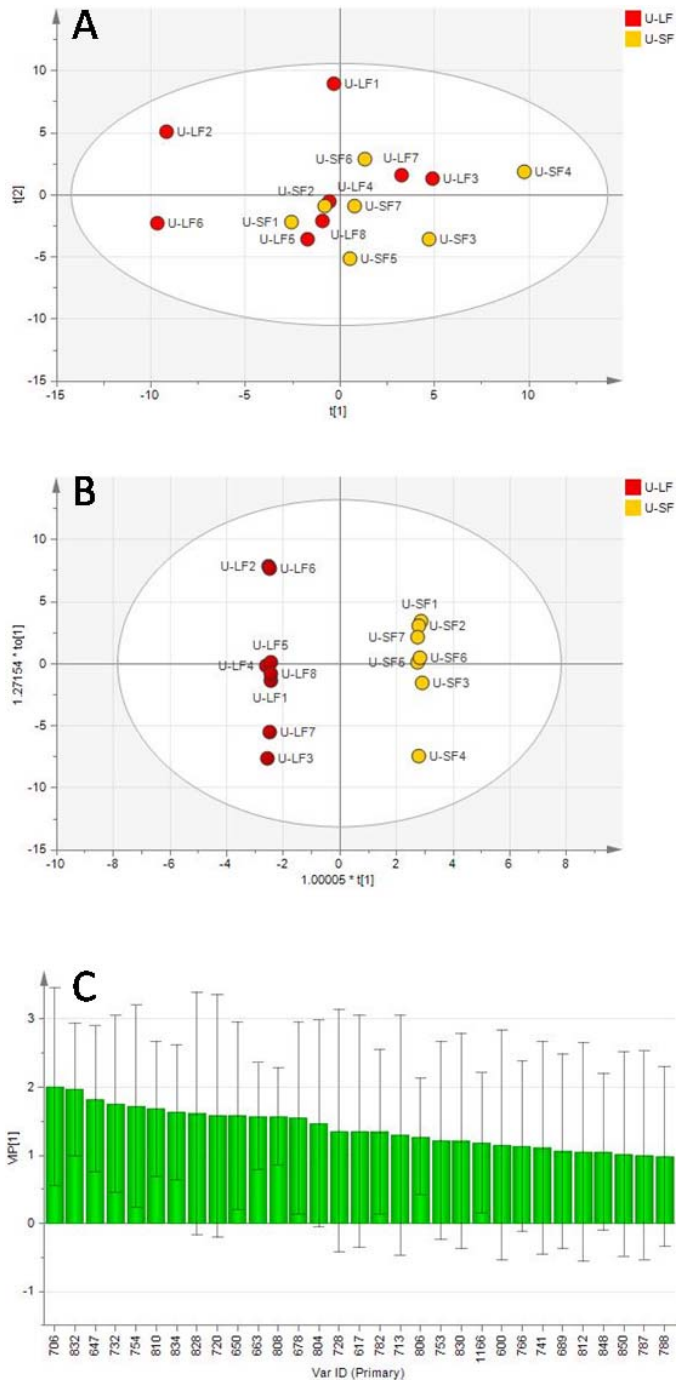


FIG. 4. A PCA (**A**) and an OPLS (**B**) plot of the MALDI(+)-MS data obtained from the uterus of cows at D4 of the estrous cycle. Each colored dot represents an individual animal of the LF-LCL (U-LF; red) or SF-SCL (U-SF; yellow) group. No discrimination of the two groups was observed ($R^2 = 0.21$) by PCA. **B**) Strong separation of the two groups was observed by OPLS ($R^2 = 0.43$; $Q^2 = 1.0$). **C**) A VIP plot with the ions responsible for the OPLS discrimination.

separation between the two animal groups (Fig. 2B). Ions of *m/z* 650.5, 703.5, 725.5, 732.6, 758.6, 760.6, 780.6, 782.6 786.6, 788.6, 808.6, and 810.6 were identified as sodiated or protonated molecules of the following lipids: SM, PC and phosphatidylethanolamines (PE), ceramides (Cer), and diacylglycerols (DG), that is: (Cer [42:1] + H)$^+$, (SM [34:1] + H)$^+$, (SM [34:1] + Na)$^+$, (PC [32:1] + H)$^+$, (PC [34:2] + H)$^+$, (PC [34:1] + H)$^+$, (PC [36:5] + H)$^+$, (PC [36:4] + H)$^+$ (PC [36:2] + H)$^+$, (PC [36:1] + H)$^+$, (PC [38:6] + H)$^+$, and (PC [38:4] + H)$^+$, respectively. Univariate analysis of the mean abundance of each of these ions showed no difference between treatments.

*Uterus D4*. The lipid profile of the uterus of LF-LCL and SF-SCL cows at D4 of the estrous cycle was also determined by MALDI-MS. Representative MALDI spectra for each experimental group are shown in Figure 3.

The profile of the uterus at D4 of the estrous cycle is characterized by the lipid ions of *m/z* 647.6, 650.6, 685.4, 703.5, 725.5, 728.6, 734.6, 758.6, 760.6, 780.6, 782.6, 786.6, 798.6, 808.6, 810.6, and 832.6, which are again attributed to sodiated or protonated molecules of SM, PC, PE, DG, and Cer. Subsequently, MALDI-MS data were explored by multivariate analysis (Fig. 4, A and B) to investigate differences between the experimental groups. In the score plot of the PCA model constructed with two principal components (Fig. 4A), no clustering was observed, R2 [cum] = 0.21. Next, an OPLS model was used to measure the multidimensional association of the lipid profile of the tissue with the endocrine phenotype provided by the biological model (i.e., LF-LCL vs. SF-SCL) and produced an R2 [cum] = 0.43 and Q2 [cum] = 1. The model was built from a single predictive and one orthogonal component, resulting in a strong separation between the two animal groups as well as little individual animal variability inside each group (Fig. 4B). In Figure 4C, the variable importance in projection (VIP) plot shows the ions responsible for the discrimination of the two groups in the OPLS model. The assignments of these ions, achieved by HRMS and database search, are reported in Table 1.

Ions of *m/z* 650.5, 720.6, 732.6, 754.6, 782.6, 804.6, 808.6, 810.6, 832.6, and 834.6 (Fig. 5) were assigned as the protonated lipids Cer (42:1), PC (31:0), PC (32:1), PC (34:4), PC (36:4), PC (38:7), PC (38:5), PC (38:4), PC (40:7), and PC (40:6), respectively. The abundances for the ions from Cer (42:1), PC (31:0), PC (32:1), and PC (34:4) were increased in the uterus of LF-LCL cows ($P < 0.05$). The phospholipid ions for PC (36:4), PC (38:7), PC (38:5), PC (38:4), PC (40:7), and PC (40:6) were more abundant in the uterus of SF-SCL cows ($P < 0.05$).

### *Experiment 2: Lipid Profile of Uterus at D7*

The lipid profile of the uterus of LF-LCL and SF-LCL cows at D7 of the estrous cycle was also investigated by MALDI-MS (Fig. 6).

The lipid profile of the bovine uterus at D7 of estrous cycle was characterized by the ions of *m/z* 647.5, 650.5, 663.5, 685.6, 703.6, 725.6, 728.6, 734.6, 741.6, 758.6, 760.6, 772.6, 782.6, 784.6, 786.6, 788.6, 798.6, 808.6, 808.6, 810.6, 824.6, 832.6, 834.6, 836.6, and 848.6, which were again identified as sodiated or protonated molecules of SM, PC, PE, Cer, and DG. Subsequently, MALDI-MS data were explored by multivariate analysis. In the score plot of the PCA model (R2 [cum] = 0.4, constructed with two principal components), two distinct clusters were observed (Fig. 7A). The principal component 1 (R2X = 0.26, t[1]) represents the variation inside each group, whereas the principal component 2 (R2X = 0.14, t[2]) is responsible for the discrimination of the two groups of samples. Next, an OPLS model was used to measure the multidimensional association of the lipid profile of the tissue with the endocrine phenotype provided by the biological model (i.e., LF-LCL vs. SF-SCL) and produced (R2 [cum] = 0.93 and Q2 [cum] = 0.9). The model was built from a single predictive and one orthogonal component, resulting in a strong separation

TABLE 1. Uterine lipids responsible for the discrimination between LF-LCL and SF-SCL cows at D4.

| Experimental *m/z*[a] | Assignments (CN:DB)[b] | Molecular formula | Accurate *m/z*[c] | Theoretical *m/z* | Error, ppm |
|---|---|---|---|---|---|
| 617.5 | [DG (36:4) + H]$^+$ | $C_{39}H_{69}O_5$ | 617.51336 | 617.5139 | −0.874 |
| 650.5 | [Cer (42:1) + H]$^+$ | $C_{42}H_{84}NO_3$ | 650.64386 | 650.6446 | −1.14 |
| 706.5 | [PC (30:0) + H]$^+$ | $C_{38}H_{77}NO_8P$ | 706.53797 | 706.5381 | −0.184 |
| 712.6 | [PC (p30:0) + H]$^+$ | $C_{38}H_{76}NO_7PNa$ | 712.52780 | 712.5252 | 3.06 |
| 720.5 | [PC (31:0) + H]$^+$ | $C_{39}H_{79}NO_8P$ | 720.55415 | 720.5538 | 0.486 |
| 728.6 | [PE (36:2) + H]$^+$ | $C_{41}H_{79}NO_7P$ | 728.55875 | 728.5589 | −0.206 |
| 732.6 | [PC (32:1) + H]$^+$ | $C_{40}H_{79}NO_8P$ | 732.55362 | 732.5538 | −0.246 |
| 752.6 | [PC (34:5)+ H]$^+$ | $C_{42}H_{75}NO_8P$ | 752.55874 | 752.5589 | −0.213 |
| 754.5 | [PC (34:4) + H]$^+$ | $C_{42}H_{77}NO_8P$ | 754.53852 | 754.5381 | −0.557 |
| 782.6 | [PC (36:4) + H]$^+$ | $C_{44}H_{81}NO_8P$ | 782.56908 | 782.5694 | −0.409 |
| 804.6 | [PC (38:7) + H]$^+$ | $C_{46}H_{79}NO_8P$ | 804.55254 | 804.5538 | −1.56 |
| 806.6 | [PC (38:6) + H]$^+$ | $C_{46}H_{81}NO_8P$ | 806.56897 | 806.5694 | 0.533 |
| 808.6 | [PC (38:5) + H]$^+$ | $C_{46}H_{83}NO_8P$ | 808.58449 | 808.5851 | 0.754 |
| 810.6 | [PC (38:4) + H]$^+$ | $C_{46}H_{85}NO_8P$ | 810.59996 | 810.6007 | −0.913 |
| 828.6 | [PC (40:9) + H]$^+$ | $C_{48}H_{79}NO_8P$ | 828.55138 | 828.5538 | −2.68 |
| 832.6 | [PC (40:7) + H]$^+$ | $C_{48}H_{83}NO_8P$ | 832.58433 | 832.5851 | −0.925 |
| 834.6 | [PC (40:6) + H]$^+$ | $C_{48}H_{85}NO_8P$ | 834.60045 | 834.6007 | −0.300 |

[a] Data acquired by MALDI(+)-TOF-MS.
[b] CN:DB, carbon number/double bound; PC, phosphatidylcholines; DG, diacylglycerols; PE, phosphoethanolamines; Cer, ceramides.
[c] Data acquired by ESI(+)-Orbitrap-MS.

between the two animal groups (Fig. 7B). The score plot shows the separation between the two groups, as well as the individual animal variability inside each group. In Figure 7C, the VIP plot shows the ions responsible for the discrimination of the two groups in the OPLS model. The assignments of these ions, achieved again by HRMS and database search, are reported in Table 2.

Lipid ions of *m/z* 701.5, 734.6, 741.6, and 772.6 (Fig. 8) were attributed to protonated or potassiated SM (34:2), PC (32:1), SM (34:1), and PC (35:2), respectively. These ions were more abundant in the LF-LCL group than in the SF-SCL group ($P < 0.05$).

### *MALDI Imaging Phospholipids*

The spatial distributions of PC and sphingomyelins in the uterus were investigated by MALDI-MS imaging. For a representative animal, Figure 9 shows the distribution of some of the lipid ions that led to discrimination of the two groups of study by univariate and multivariate analysis. The initial goal was to compare the abundance of specific lipid ions on specific compartments between the experimental groups. We noted, as expected, large among-animal variability within each group regarding ion abundance (data not shown), but tissue distribution of each lipid ion showed unique patterns. For example, SM (34:1) showed greatest abundance on the myometrial layer, whereas PC (35:2) showed a clear accumulation associated with the luminal epithelium of the endometrium. In contrast, ions for PC (38:7), PC (38:5), and PC (38:4) showed a great accumulation on the uterus region in comparison with the myometrium. Finally, SM (34:2), PC (31:0), PC (32:0), PC (40:7), and PC (40:6) showed a diffused pattern of uterine distribution.

## DISCUSSION

In cattle, the first week after estrus is critical for a successful gestation. During this short window, sequential reproductive events take place in the oviduct and uterus, such as sperm and oocyte transport, fertilization, initial cleavages of the embryo, and subsequent blastocyst formation. In vivo, all such processes depend on successful interactions with the reproductive tract. Function of the reproductive tract is controlled by fluctuations of the concentrations of sex steroids that occur during the periovulatory period, specifically E2 during the proestrus and estrus and P4 during the early diestrus. These hormones act through their nuclear and membrane receptors to change transcription and protein synthesis in target tissues. Global transcriptome and proteome changes induced by sex steroids in the uterus and oviduct have been reported extensively, but global changes in metabolites, such as carbohydrates and lipids, need characterization. For example, phospholipids are vital structural and regulatory components of biological membranes and serve as precursors for many active biomolecules, such as eicosanoids and lysophospholipids [15, 16]. Lipids are also involved in signaling pathways [26, 29–31]. In cattle, lipid profiles of the reproductive tract are not well characterized, despite the evidence that phospholipid metabolism and signaling influence early pregnancy events [32]. Indeed, the profiles of PC and SM are distinctly different between bovine embryos produced in vivo (greater chance of pregnancy success) versus those produced in vitro (poorer chance of pregnancy success) [22, 33]. Specifically, passage through the reproductive tract dictates changes in the molecular composition of the embryo. This finding provides indirect evidence that embryo development past the blastocyst stage is influenced by the biochemical milieu to which it is exposed during development to the blastocyst stage. Here, we have collected data on the nature and abundance of the main phospholipids present in the bovine oviduct and uterus at the first week after estrus. Most importantly, we showed that such molecules were regulated by the periovulatory endocrine milieus associated with poor (SF-SCL group) or good (LF-LCL) receptivity and fertility. Phospholipid characterization was achieved by MALDI-MS using high resolution and accuracy in an Orbitrap mass spectrometer, followed by tandem MS/MS and database search.

If a cow is inseminated, it is expected that on D4 the embryo will be in the oviduct, probably in transit between the isthmus and the uterus [34]. Our recent work [35] showed clearly that there are dramatic changes both in the ampullar and isthmic transcriptomes of tissues collected from the same cows used in the present study. Such changes are regulated by the distinctly different concentrations of E2 during the proestrus and estrus and P4 during the early diestrus, as well as their respective nuclear and membrane receptors [35]. Accordingly, we expected that the phospholipid profile would also differ

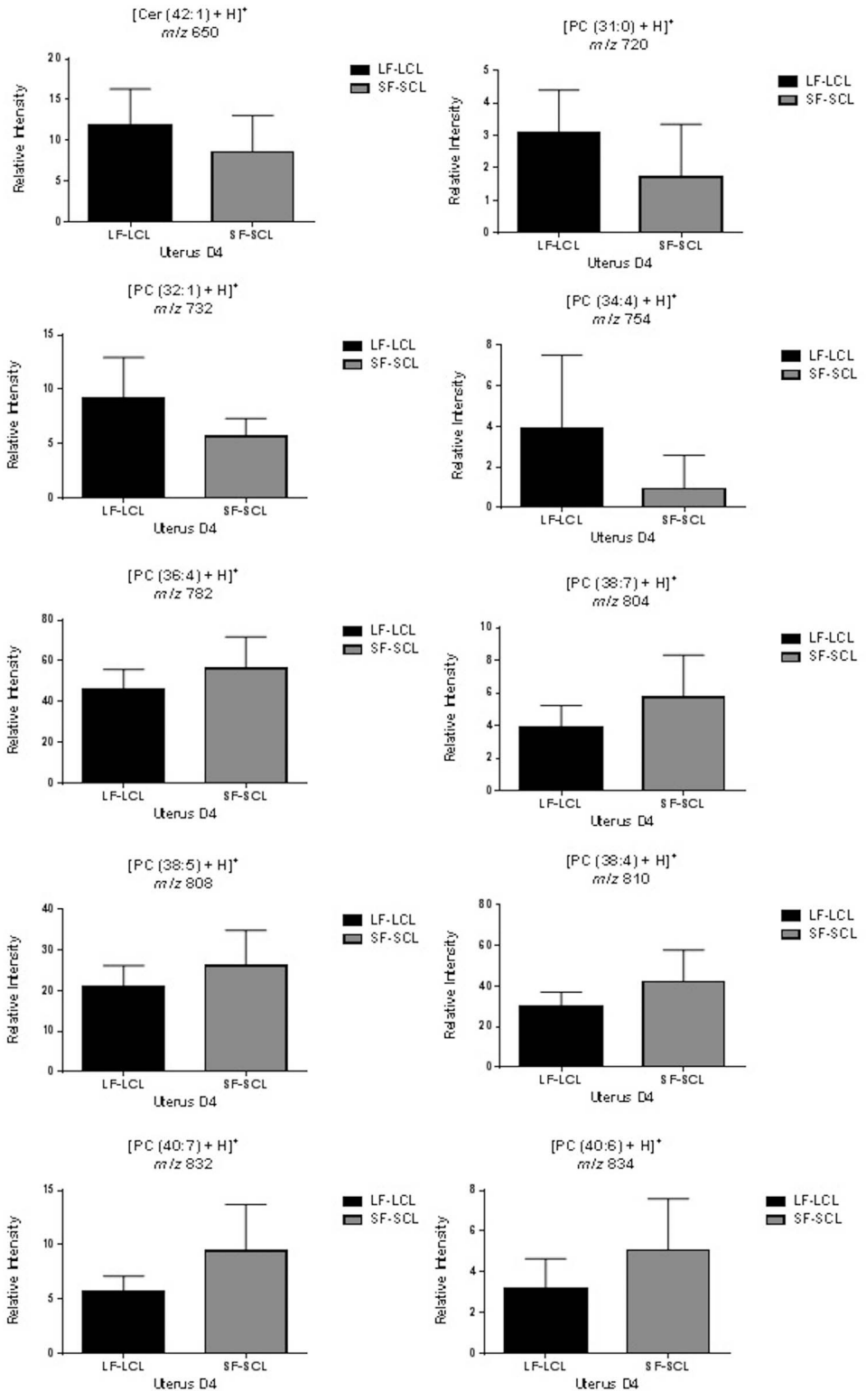


FIG. 5. Changes in the relative abundance of lipids in bovine uterus from LF-LCL and SF-SCL cows at D4 of the estrous cycle. Treatment means differed for all lipids ($P < 0.05$).

between treatments. The MALDI-MS data show that the phospholipid profile of the oviduct at D4 is mainly characterized by a complex mixture of several unsaturated phospholipids. Multivariate analysis, however, failed to indicate a clear clustering of animals of the same experimental group according to the lipid profile. This finding suggests that lipid profiles in the oviduct vary in a nonuniform fashion among individuals in response to the periovulatory endocrine milieu differences evoked by the ovulation of different-sized follicles. It also may be speculated that there is not a clear phospholipid profile

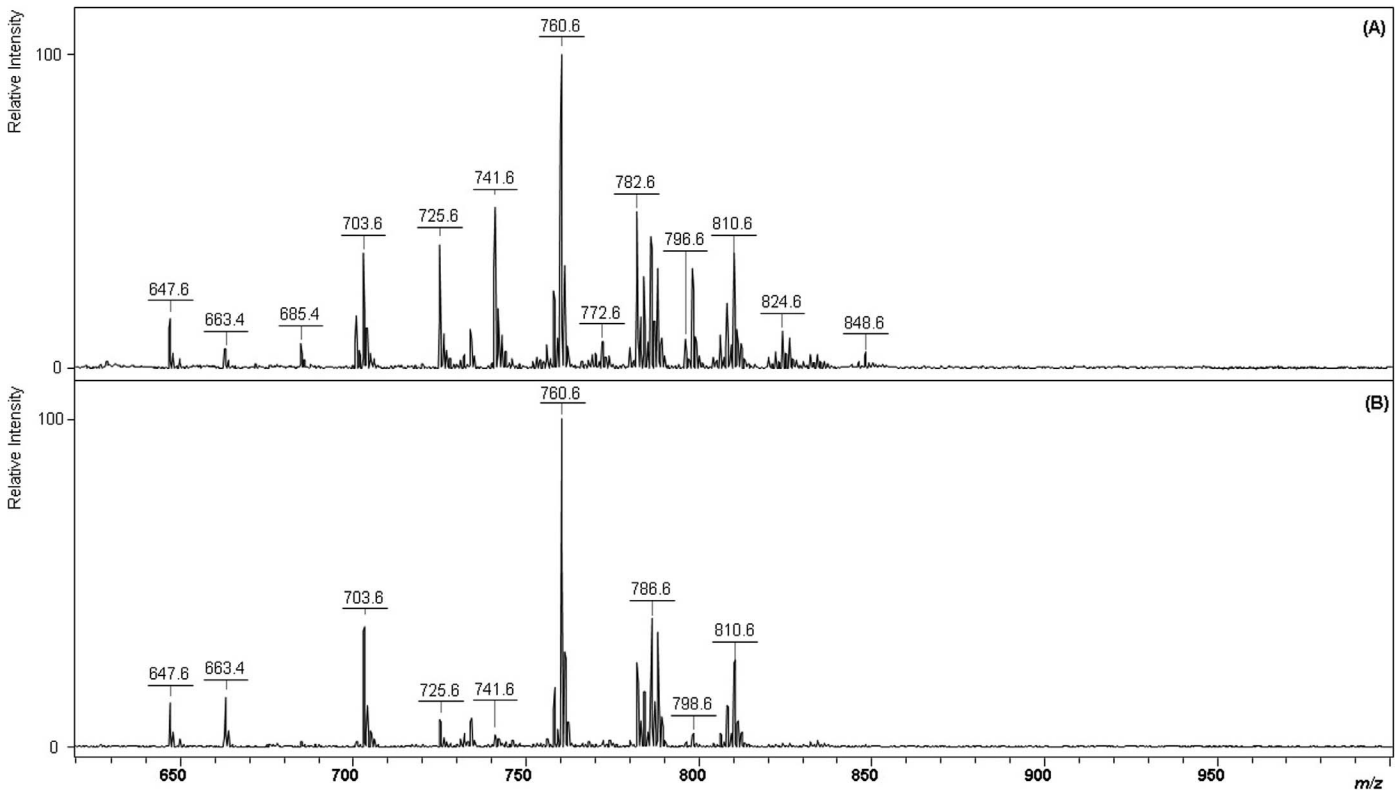


FIG. 6. Representative MALDI(+)-MS of the uterus of (A) LF-LCL and (B) SF-SCL cows at D7 of the estrous cycle. The x-axis represents the *m/z* values of lipid ions, whereas the y-axis reports the relative abundance of each ion expressed as a percentage to the most abundant ion.

associated with oviductal functions that modulate receptivity on D4.

On D4 the uterus is preparing to receive the embryo that will be transported from the oviduct in the next 12 to 24 h. Similar to the oviduct, this organ was exposed to the different sex steroid milieus associated with the ovulation of different sizes of follicles on the SF-SCL and LF-LCL groups. Our unpublished data also indicate that the expression of both sex steroid receptors and uterus genes was different between groups. Again, we hypothesized that phospholipid profiles would respond to the distinct sex steroid tones provided by hormones and their cognate receptors. The MALDI-MS data show that phospholipid profile of uterus at D4 is again characterized by a complex mixture of unsaturated phospholipids. Multivariate analyses, especially the OPLS (Fig. 4B), clearly separated the two populations of individuals according to the two distinct treatments. Analysis of the lipid ions mainly contributing to the separation between groups detected one Cer (42:1) and three species of PC (31:0, 32:1, and 34:4) that were more abundant in the LF-LCL group, whereas six ions associated with higher-MW PC (36:4, 38:7, 38:5, 38:4, 40:7, and 40:6) had reduced abundance in that group. We can interpret this finding as evidence that a defined profile of phospholipids is generated when the uterus is exposed to distinctly different periovulatory endocrine milieus. Limited information is available on the effects of periovulatory steroids in the phospholipid composition of the bovine reproductive tract. However, these molecules clearly modulate phospholipid abundance and function in other models. For example, in breast cancer, synthesis of Cer is stimulated by estradiol [36]. Abundance of Cer has also been associated positively with apoptosis [13, 37], and our data showed that cows in the LF-LCL group presented a greater proportion of apoptotic cells in the endometrium compared with the SF-SCL group on D7 of the estrous cycle [12, 13, 27]. It is therefore plausible to propose that elevated proestrus-estrus estradiol concentrations stimulated Cer on D4 to induce a greater proportion of apoptotic cells on D7. As discussed by Mesquita et al. [13], an increased apoptotic, decreased proliferative phenotype may be required for embryo receptivity. Furthermore, Cer seem also to be essential for embryo development. Ceramide transferase gene (*CERT*) mutant mouse embryos showed impaired cell proliferation [38].

Another group of phospholipids modulated by our model on D4 was the PC. In the rat, production of PC is stimulated by estradiol in bones, whereas in rabbits, this steroid stimulates PC in the fetal lung [39, 40]. In addition, the PC (32:1), which is more abundant in endometrium of cows from the LF-LCL group on D4 and D7, is also more abundant in embryos produced in vivo compared with embryos obtained from in vitro production (IVP) [22]. In contrast, PC (38:4), which is more abundant in the SF-SCL group, is more abundant in IVP embryos compared with in vivo-produced embryos [22]. Collectively, it is possible that both the endometrium and the embryo benefit from changes in the abundance of Cer and PC caused by different periovulatory endocrine milieus.

The pregnant endometrium on D7 must provide physical and biochemical support to the blastocyst, which is free-floating and must rely on molecules present in the uterine lumen for nutrients and growth factor support. The periovulatory endocrine milieu directly impacts the uterine function to support embryo development. Indeed, we deciphered the endometrium transcriptome of cows treated to ovulate larger (LF-LCL group) or smaller (SF-SCL group) follicles and

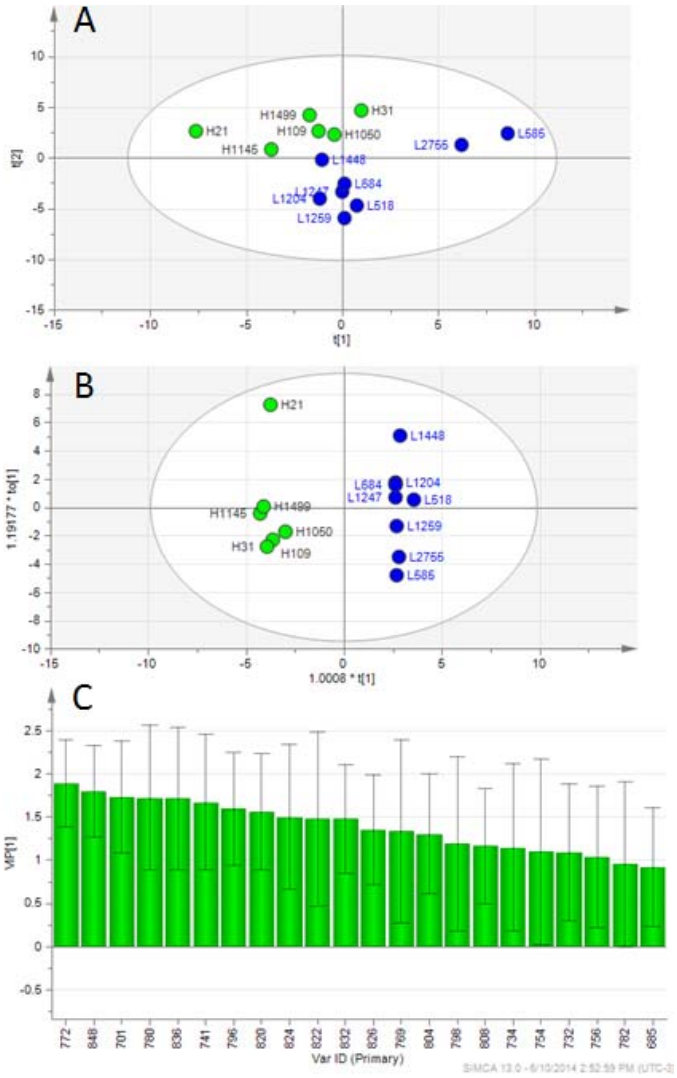


FIG. 7. A PCA (**A**) and an OPLS (**B**) plot of the MALDI (+)-MS data obtained from the uterus of LF-LCL or SF-SCL cows at D7 of the estrous cycle. Each colored dot represents an individual animal of the LF-LCL (L; blue) or SF-SCL (S; green) group. A weak discrimination of the two groups was observed ($R^2 = 0.4$) by PCA. **B**) Strong separation of the two groups was observed by OPLS ($R^2 = 0.93$; $Q^2 = 0.9$). **C**) A VIP plot with the ions responsible for the OPLS discrimination.

TABLE 2. Uterine lipids responsible for the discrimination between LF-LCL and SF-SCL cows at D7.

| Experimental $m/z$[a] | Assignments (CN:DB)[b] | Molecular formula | Accurate $m/z$[c] | Theoretical $m/z$ | Error, ppm |
|---|---|---|---|---|---|
| 701.6 | $[SM\ (34:2) + H]^+$ | $C_{39}H_{78}N_2O_6P$ | 701.55894 | 701.5592 | −0.371 |
| 732.6 | $[PC\ (32:1) + H]^+$ | $C_{40}H_{79}NO_8P$ | 732.55362 | 732.5538 | −0.246 |
| 734.6 | $[PC\ (32:0) + H]^+$ | $C_{40}H_{81}NO_8P$ | 734.56943 | 734.5694 | 0.041 |
| 741.6 | $[SM\ (34:1) + K]^+$ | $C_{39}H_{79}N_2O_6PK$ | 741.52972 | 741.5307 | −1.322 |
| 754.5 | $[PC\ (34:4) + H]^+$ | $C_{42}H_{77}NO_8P$ | 754.53852 | 754.5381 | −0.557 |
| 756.6 | $[PC\ (34:3) + H]^+$ | $C_{42}H_{79}NO_8P$ | 756.55370 | 756.5538 | −0.132 |
| 768.6 | $[PC\ (35:4) + H]^+$ | $C_{43}H_{79}NO_8P$ | 768.55384 | 768.5538 | 0.052 |
| 772.6 | $[PC\ (35:2) + H]^+$ | $C_{43}H_{83}NO_8P$ | 772.58490 | 772.5851 | −0.259 |
| 780.6 | $[PC\ (36:5) + H]^+$ | $C_{44}H_{79}NO_8P$ | 780.55343 | 780.5538 | −0.474 |
| 782.6 | $[PC\ (36:4) + H]^+$ | $C_{44}H_{81}NO_8P$ | 782.56908 | 782.5694 | −0.409 |
| 796.6 | $[PC\ (37:4) + H]^+$ | $C_{45}H_{83}NO_8P$ | 796.58492 | 796.5851 | −0.226 |
| 798.6 | $[PC\ (37:3) + H]^+$ | $C_{45}H_{85}NO_8P$ | 798.60119 | 798.6007 | 0.614 |
| 804.6 | $[PC\ (38:7) + H]^+$ | $C_{46}H_{79}NO_8P$ | 804.55254 | 804.5538 | −1.566 |
| 808.6 | $[PC\ (38:5) + H]^+$ | $C_{46}H_{83}NO_8P$ | 808.58449 | 808.5851 | −0.754 |
| 820.6 | $[PC\ (39:6) + H]^+$ | $C_{47}H_{83}NO_8P$ | 820.58478 | 820.5851 | −0.390 |
| 822.6 | $[PC\ (39:5) + H]^+$ | $C_{47}H_{85}NO_8P$ | 822.60055 | 822.6007 | −0.182 |
| 824.6 | $[PC\ (36:2) + K]^+$ | $C_{44}H_{84}NO_8PK$ | 824.55630 | 824.5566 | −0.364 |
| 826.6 | $[PC\ (36:1) + K]^+$ | $C_{44}H_{86}NO_8PK$ | 826.57203 | 826.5723 | −0.327 |
| 832.6 | $[PC\ (40:7) + H]^+$ | $C_{48}H_{83}NO_8P$ | 832.58433 | 832.5851 | −0.925 |
| 836.6 | $[PC\ (40:5) + H]^+$ | $C_{48}H_{87}NO_8P$ | 836.61620 | 836.6164 | −0.239 |
| 848.6 | $[PC\ (38:4) + K]^+$ | $C_{46}H_{84}NO_8PK$ | 848.55619 | 848.5566 | −0.483 |

[a] Data acquired by MALDI(+)-TOF-MS.
[b] CN:DB, carbon number/double bound; PC, phosphatidylcholines; SM, sphingomyelins.
[c] Data acquired by ESI(+)-Orbitrap-MS.

reported clear differences between groups [13]. For example, the LF-LCL group, associated with greater fertility [4], presented less proliferation, more apoptosis, and a greater capacity to control oxidative stress compared with the SF-SCL group [13]. To the best of our knowledge, this is the first report on the endometrium metabolome in cattle. Resolution of the profiles shown in Figure 7 revealed that the phospholipid profile of uterus at D7 is characterized again by a complex mixture of several unsaturated phospholipids, mainly PC with contrasting MW. Similar to D4, the OPLS analysis was highly discriminatory (Fig. 8B). Lipids that mostly contributed to group separation were SM (34:1), SM (34:2), PC (32:1), and PC (35:2), which were all relatively more abundant in the LF-LCL group. Regarding PC (35:2), it showed abundant and specific localization to the luminal epithelium (Fig. 9). Because of spatial proximity to an eventual embryo, it is tempting to speculate on a functional role for this phospholipid in embryo development. Lipid-specific functions on receptivity, however, are largely unknown to this point.

The increased abundance of SM (34:1) and SM (34:2) in the endometrium of group LF-LCL suggests that SM-mediated signaling occurred at D7. Besides a structural function as a bilayer-stabilizing lipid, SM fulfills an important role as the precursor for the lipid second messenger Cer in the so-called sphingomyelin cycle [41, 42]. One important step in SM metabolism is the phosphorylation of SM to sphingosine 1-phosphate by sphingosine kinases. The SM plays a pivotal role in the early stage of pregnancy. For example, disturbance in sphingolipid metabolism in mice by disruption of sphingosine kinase genes causes sphingoid base accumulation, and consequently early pregnancy loss. This loss was mainly due to a compromised decidualization and uterine vascular instability [43]. Conversely, both pregnancy and progesterone supplementation in rats stimulated the expression of sphingosine kinase-1 gene in the uterus, which was essential to growth and differentiation to support pregnancy [44]. Supplementation of conjugated linoleic acid during embryo production in vitro was also found to increase embryo SM and PC abundance, and improved embryo quality and survival after cryopreservation [33]. The increased abundance of SM species in the uterus of LF-LCL cows is therefore consistent with the greater concentrations of progesterone in this group, and also with the potentially positive effects of this phospholipid to uterine receptivity to the embryo.

Successful preimplantation embryo development depends on reproductive tract composition and function. Here, for the first time, we used high-accuracy and high-resolution MALDI-MS to comprehensively characterize the global phospholipid

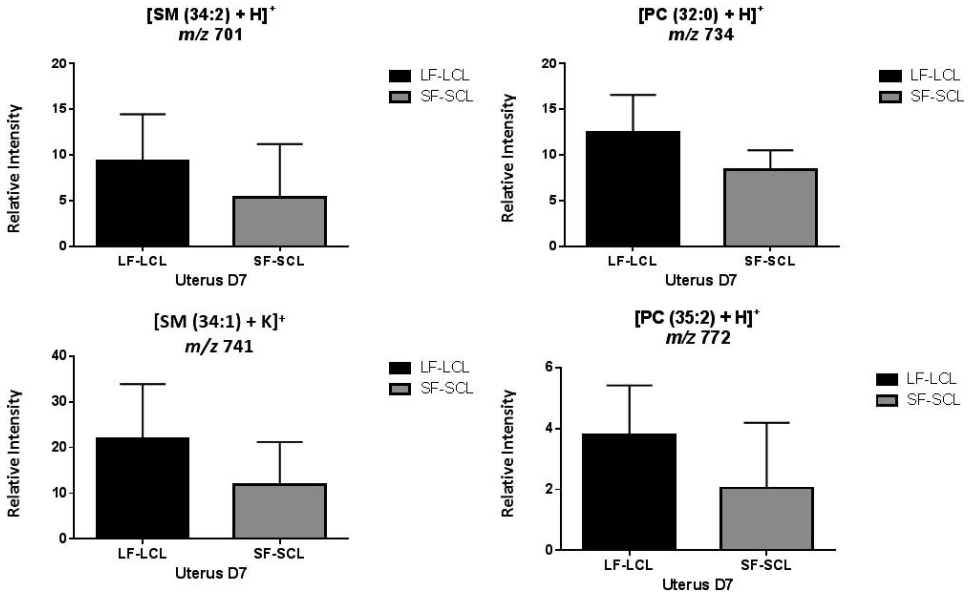


FIG. 8. Changes in the relative abundance of lipids present in the bovine uterus of LF-LCL and SF-SCL cows at D7 of the estrous cycle. Treatment means differed for all lipids ($P < 0.05$).

composition of the oviduct and the uterus at the beginning of the estrous cycle. More importantly, we showed that global and specific phospholipid abundance is modulated by periovulatory endocrine milieus associated with poor (SF-SCL) versus greater (LF-LCL) receptivity. Specific PC, PE, SM, and Cer abundances varied according to treatments. Functional studies specifically designed to interrogate the role of phospholipids on uterine function and embryo development are warranted. A proper assessment of phospholipid composition in the reproductive tract should contribute to critically increase the understanding of their role in bovine preimplantation reproductive tract biology.

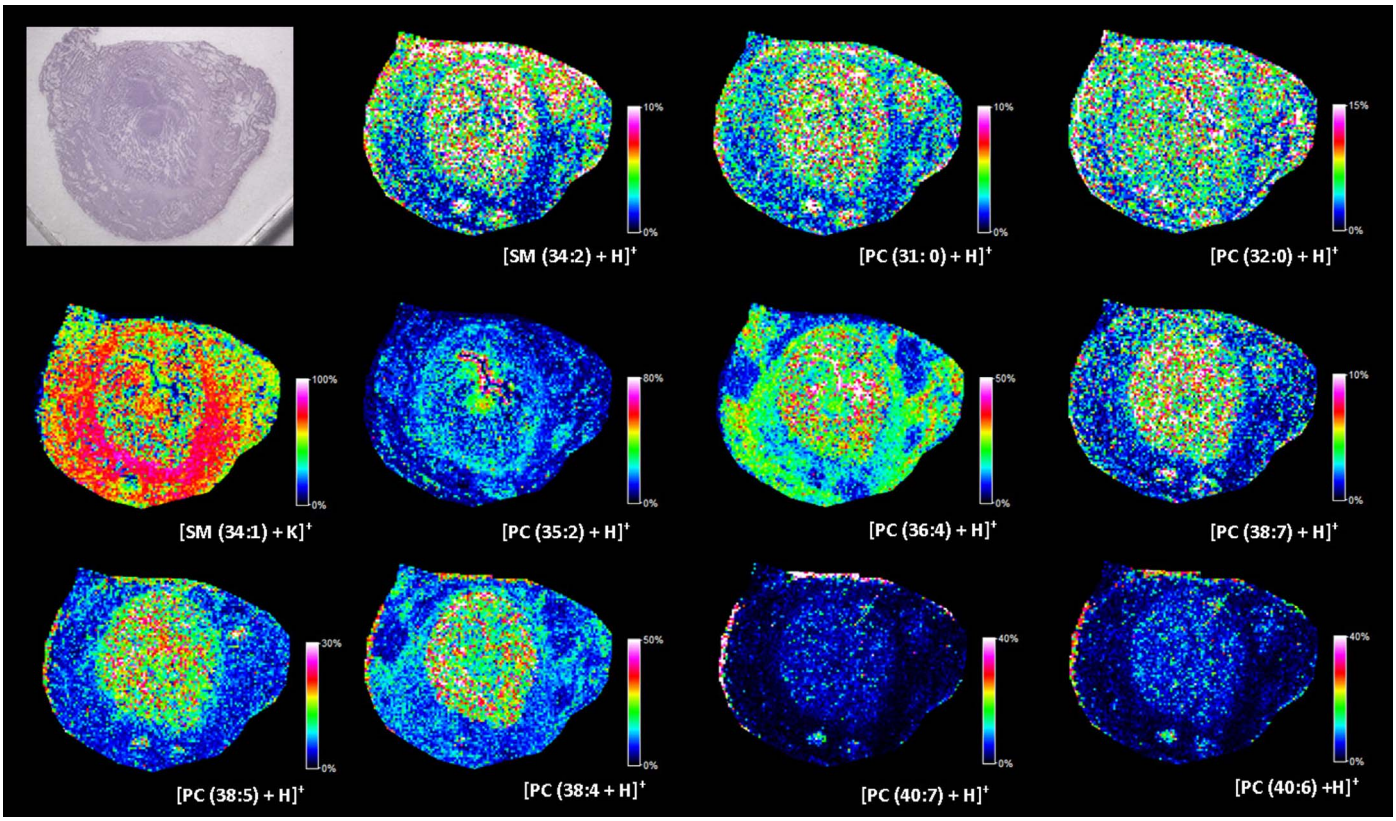


FIG. 9. An optical image of hematoxylin-eosin-stained cow uterus section (top left) and MALDI-MS ion images of the most relevant phospholipid ions in the uterus. Blue, green, and red tones represent low, medium, and elevated relative abundance of each phospholipid ion for PC and SM.

## REFERENCES


1. Santos JE, Thatcher WW, Chebel RC, Cerri RL, Galvao KN. The effect of embryonic death rates in cattle on the efficacy of estrus synchronization programs. Anim Reprod Sci 2004; 83:513–535.
2. Binelli M, Machado R, Bergamaschi MACM, Bertan CM. Manipulation of ovarian and uterine function to increase conception rates in cattle. Anim Reprod 2009; 6:125–134.
3. Diskin MG, Morris DG. Embryonic and early foetal losses in cattle and other ruminants. Reprod Domest Anim 2008; 43:260–267.
4. Pugliesi G, Santos FB, Lopes E, Nogueira E, Maio JR, Binelli M. Improved fertility in suckled beef cows ovulating large follicles or supplemented with long-acting progesterone after timed-AI. Theriogenology 2016; 85:1239–1248.
5. Lonergan P, O'Hara L, Forde N. Role of diestrus progesterone on endometrial function and conceptus development in cattle. Anim Reprod 2013; 10:223–227.
6. Thatcher WW, Guzeloglu A, Mattos R, Binelli M, Hansen TR, Pru JK. Uterine-conceptus interactions and reproductive failure in cattle. Theriogenology 2001; 56:1435–1450.
7. Binelli M, Thatcher WW, Mattos R, Baruselli PS. Antiluteolytic strategies to improve fertility in cattle. Theriogenology 2001; 56:1451–1463.
8. Demetrio DGB, Santos RM, Demetrio CGB, Vasconcelos JLM. Factors affecting conception rates following artificial insemination or embryo transfer in lactating holstein cows. J Dairy Sci 2007; 90:5073–5082.
9. Meneghetti M, Sa Filho OG, Peres RFG, Lamb GC, Vasconcelos JLM. Fixed-time artificial insemination with estradiol and progesterone for *Bos indicus* cows I: basis for development of protocols. Theriogenology 2009; 72:179–189.
10. Peres RFG, Claro I Jr, Sa Filho OG, Nogueira GP, Vasconcelos JLM. Strategies to improve fertility in *Bos indicus* postpubertal heifers and nonlactating cows submitted to fixed-time artificial insemination. Theriogenology 2009; 72:681–689.
11. Frade MC, Frade C, Cordeiro MB, Sá Filho MF, Mesquita FS, Nogueira GdP, Binelli M, Membrive CMB. Manifestation of estrous behavior and subsequent progesterone concentration at timed-embryo transfer in cattle are positively associated with pregnancy success of recipients. Anim Reprod Sci 2014; 151:85–90.
12. Mesquita FS, Pugliesi G, Scolari SC, Franca MR, Ramos RS, Oliveira M, Papa PC, Bressan FF, Meirelles FV, Silva LA, Nogueira GP, Membrive CM, et al. Manipulation of the periovulatory sex steroidal milieu affects endometrial but not luteal gene expression in early diestrus Nelore cows. Theriogenology 2014; 81:861–869.
13. Mesquita FS, Ramos RS, Pugliesi G, Andrade SC, Van Hoeck V, Langbeen A, Oliveira ML, Gonella-Diaza AM, Gasparin G, Fukumasu H, Pulz LH, Membrive CM, et al. The receptive endometrial transcriptomic signature indicates an earlier shift from proliferation to metabolism at early diestrus in the cow. Biol Reprod 2015; 93:52.
14. Ramos RS, Oliveira ML, Izaguirry AP, Vargas LM, Soares MB, Mesquita FS, Santos FW, Binelli M. The periovulatory endocrine milieu affects the uterine redox environment in beef cows. Reprod Biol Endocrinol 2015; 13:39.
15. Khan WA, Blobe GC, Hannun YA. Arachidonic acid and free fatty acids as second messengers and the role of protein kinase C. Cell Signal 1995; 7:171–184.
16. Mills GB, Moolenaar WH. The emerging role of lysophosphatidic acid in cancer. Nat Rev Cancer 2003; 3:582–591.
17. Meier S, Trewhella MA, Fairclough RJ, Jenkin G. Changes in uterine endometrial phospholipids and fatty acids throughout the oestrous cycle and early pregnancy in the ewe. Prostaglandins Leukot Essent Fatty Acids 1997; 57:341–349.
18. Burlingame AL, Boyd RK, Gaskell SJ. Mass spectrometry. Anal Chem 1998; 70:647R–716R.
19. Ferreira CR, Saraiva SA, Catharino RR, Garcia JS, Gozzo FC, Sanvido GB, Santos LF, Lo Turco EG, Pontes JH, Basso AC, Bertolla RP, Sartori R, et al. Single embryo and oocyte lipid fingerprinting by mass spectrometry. J Lipid Res 2010; 51:1218–1227.
20. Tata A, Sudano MJ, Santos VG, Landim-Alvarenga FD, Ferreira CR, Eberlin MN. Optimal single-embryo mass spectrometry fingerprinting. J Mass Spectrom 2013; 48:844–849.
21. Apparicio M, Ferreira CR, Tata A, Santos VG, Alves AE, Mostachio GQ, Pires-Butler EA, Motheo TF, Padilha LC, Pilau EJ, Gozzo FC, Eberlin MN, et al. Chemical composition of lipids present in cat and dog oocyte by matrix-assisted desorption ionization mass spectrometry (MALDI- MS). Reprod Domest Anim 2012; 6:113–117.
22. Sudano MJ, Santos VG, Tata A, Ferreira CR, Paschoal DM, Machado R, Buratini J, Eberlin MN, Landim-Alvarenga FD. Phosphatidylcholine and sphingomyelin profiles vary in *Bos taurus indicus* and *Bos taurus taurus* in vitro- and in vivo-produced blastocysts. Biol Reprod 2012; 87:130.
23. Fuchs B, Jakop U, Goritz F, Hermes R, Hildebrandt T, Schiller J, Muller K. MALDI-TOF ''fingerprint'' phospholipid mass spectra allow the differentiation between ruminantia and feloideae spermatozoa. Theriogenology 2009; 71:568–575.
24. Schiller J, Muller K, Suss R, Arnhold J, Gey C, Herrmann A, Lessig J, Arnold K, Muller P. Analysis of the lipid composition of bull spermatozoa by MALDI-TOF mass spectrometry–a cautionary note. Chem Phys Lipids 2003; 126:85–94.
25. Lessig J, Gey C, Suss R, Schiller J, Glander HJ, Arnhold J. Analysis of the lipid composition of human and boar spermatozoa by MALDI-TOF mass spectrometry, thin layer chromatography and 31P NMR spectroscopy. Comp Biochem Physiol B Biochem Mol Biol 2004; 137:265–277.
26. Burnum KE, Cornett DS, Puolitaival SM, Milne SB, Myers DS, Tranguch S, Brown HA, Dey SK, Caprioli RM. Spatial and temporal alterations of phospholipids determined by mass spectrometry during mouse embryo implantation. J Lipid Res 2009; 50:2290–2298.
27. Franca MR, Mesquita FS, Lopes E, Pugliesi G, Van Hoeck V, Chiaratti MR, Membrive CB, Papa PC, Binelli M. Modulation of periovulatory endocrine profiles in beef cows: consequences for endometrial glucose transporters and uterine fluid glucose levels. Domest Anim Endocrinol 2015; 50:83–90.
28. Bligh EG, Dyer WJ. A rapid method of total lipid extraction and purification. Can J Biochem Physiol 1959; 37:911–917.
29. Hannun YA, Obeid LM. Principles of bioactive lipid signalling: lessons from sphingolipids. Nat Rev Mol Cell Biol 2008; 9:139–150.
30. Ye X, Hama K, Contos JJ, Anliker B, Inoue A, Skinner MK, Suzuki H, Amano T, Kennedy G, Arai H, Aoki J, Chun J. LPA3-mediated lysophosphatidic acid signalling in embryo implantation and spacing. Nature 2005; 435:104–108.
31. Di Paolo G, De Camilli P. Phosphoinositides in cell regulation and membrane dynamics. Nature 2006; 443:651–657.
32. Shah BH, Catt KJ. Roles of LPA3 and COX-2 in implantation. Trends Endocrinol Metab 2005; 16:397–399.
33. Leao BCS, Rocha-Frigoni NAS, Cabral EC, Coelho MB, Ferreira CR, Eberlin MN, Accorsi MF, Nogueira E, Mingoti GZ. Improved embryonic cryosurvival observed after in vitro supplementation with conjugated linoleic acid is related to changes in the membrane lipid profile. Theriogenology 2015; 84:127–136.
34. Kolle S, Dubielzig S, Reese S, Wehrend A, Konig P, Kummer W. Ciliary transport, gamete interaction, and effects of the early embryo in the oviduct: ex vivo analyses using a new digital videomicroscopic system in the cow. Biol Reprod 2009; 81:267–274.
35. Binelli M, Pugliesi G, Van Hoeck V, Sponchiado M, Ramos RS, Oliveira ML, França MR, D'Alexandri FL, Mesquita FS, Membrive CMB. The role of proestrus on fertility and postovulatory uterine function in the cow. Anim Reprod 2014; 11:246–253.
36. Wegner MS, Wanger RA, Oertel S, Brachtendorf S, Hartmann D, Schiffmann S, Marschalek R, Schreiber Y, Ferreiros N, Geisslinger G, Grosch S. Ceramide synthases CerS4 and CerS5 are upregulated by 17beta-estradiol and GPER1 via AP-1 in human breast cancer cells. Biochem Pharmacol 2014; 92:577–589.
37. Pettus BJ, Chalfant CE, Hannun YA. Ceramide in apoptosis: an overview and current perspectives. Biochim Biophys Acta 2002; 1585:114–125.
38. Wang X, Rao RP, Kosakowska-Cholody T, Masood MA, Southon E, Zhang H, Berthet C, Nagashim K, Veenstra TK, Tessarollo L, Acharya U, Acharya JK. Mitochondrial degeneration and not apoptosis is the primary cause of embryonic lethality in ceramide transfer protein mutant mice. J Cell Biol 2009; 184:143–158.
39. Cruess RL, Hong KC, Lida K. Effect of estrogen on the phospholipid metabolism of rat bone. Endocrinology 1973; 92:961–963.
40. Khosla SS, Gobran LI, Rooney SA. Stimulation of phosphatidylcholine synthesis by 17 beta-estradiol in fetal rabbit lung. Biochim Biophys Acta 1980; 617:282–290.
41. Hannun YA, Obeid LM. Ceramide - an intracellular signal for apoptosis. Trends Biochem Sci 1995; 20:73–77.
42. Kolesnick R, Fuks Z. Ceramide - a signal for apoptosis or mitogenesis. J Exp Med 1995; 181:1949–1952.
43. Mizugishi K, Li C, Olivera A, Bielawski J, Bielawska A, Deng CX, Proia RL. Maternal disturbance in activated sphingolipid metabolism causes pregnancy loss in mice. J Clin Invest 2007; 117:2993–3006.
44. Jeng YJ, Suarez VR, Izban MG, Wang HQ, Soloff MS. Progesterone-induced sphingosine kinase-1 expression in the rat uterus during pregnancy and signaling consequences. Am J Physiol Endocrinol Metab 2007; 292:E1110–E1121.